JOURNAL OF WATER AND LAND DEVELOPMENT
e-ISSN 2083-4535
Polish Academy of Sciences (PAN) Institute of Technology and Life Sciences – National Research Institute (ITP – PIB)

JOURNAL OF WATER AND LAND DEVELOPMENT
DOI: 10.24425/jwld.2026.157826
2026, No. 68 (I–III): 95–103

# Three-dimensional flow modelling of spillway chute flows for predicting cavitation potential

Marojahan L. Gaol[1)] ✉, Pitojo T. Juwono[2)] ✉, Very Dermawan[2)] ✉, Dian Sisinggih[2)] ✉, Lily M. Limantara*[2)] ✉

[1)] University of Brawijaya, Doctoral Program in Department of Water Resources, Faculty of Engineering, Jl. MT Haryono No. 167, 65145 Malang, Indonesia

[2)] University of Brawijaya, Faculty of Engineering, Department of Water Resources, Jl. MT Haryono No. 167, 65145 Malang, Indonesia

* Corresponding author

RECEIVED 21.09.2025 ACCEPTED 26.11.2025 AVAILABLE ONLINE 02.03.2026

**Abstract:** This research intends to build a 3-D flow model of a section of the spillway chute at Tigadihaji Dam under the spillway design flood with a 1000-year return period, to investigate flow behaviour and the potential of cavitation damage using a numerical model in Ansys Fluent. The numerical model is validated against a physical model, and the impact of the aerator on the chute is also assesses. The research parameters are velocity, pressure, and cavitation number, obtained from the measurements at 16 points along the chute. The methodology consists of modelling and validation. The modelling was carried out for the chute and the chute with an aerator. The validation of computational fluid dynamics (CFD) model, based on pressure data, produced a determination coefficient ($R^2$) of about 0.97. It shows that the CFD model is very good in presenting the trend and fluctuation of physical data. The cavitation analysis at $Q_{1000}$ indicates a moderate risk in chuteway-3 and a high risk in chuteway-4. To mitigate this, a deflector–offset aerator was installed at the slope transition from 1:35 to 1:1.5. The simulation results reveal an increase of up to 0.1 in the cavitation index, with improvements extending about 20 m downstream of the aerator. Nevertheless, the offset section on the milder curved profile limited performance due to incomplete aeration.

**Keywords:** aerator, cavitation, chute, computational fluid dynamics (CFD), modelling

## INTRODUCTION

The spillway channel is one of the dam appurtenant structures that plays a major role in dam safety. Its function is to maintain the flood water level so that is does not overtop the dam crest (Pfister, Hager and Asce, 2010; Bai *et al.*, 2019). If the water level exceeds the reservoir crest level, water will overflow through the spillway channel (Luna-Bahena *et al.*, 2018; Ebrahimnezhadian and Manafpour, 2021). Therefore, the spillway channel must have enough capacity (Safiloo *et al.*, 2025; Trinh *et al.*, 2025) to convey the design flood corresponding to the return period required by the design criteria. To ensure safety, some dams are equipped with auxiliary or emergency spillways (Julien, Kositgittiwong and Chinnarasri, 2014; Zhang *et al.*, 2024), which are used only under extreme conditions. Such spillways may be allowed to sustain structure damage after the passage of flood discharge (Departemen Pekerjaan Umum, Direktorat Jenderal Pengairan, Direktorat Bina Teknik, 1999; Nasrabadi and Aminpour, 2020). Therefore, maintaining the performance of the spillway channel is important to ensure proper hydraulic function (Amador, Sánchez-Juny and Dolz, 2006; Kumcu, 2017) as well as structural performance (Seo *et al.*, 2016; Kubrak and Kubrak, 2022; Kubrak, Kubrak and Binio, 2024) throughout the reservoir lifetime. Reinforced concrete is commonly used for spillway channels because it performs well hydraulically, provides favourable flow conditions, and is easy to construct.

Generally, a spillway system consists of several structural components (Yang, Teng and Zhang, 2018; Environment Agency, 2022), including the approach channel, spillway crest, chute, energy dissipator, and end channel. These components produce different flow regimes: 1) sub-critical flow in the approach channel; 2) a transition from critical to super-critical flow over

the crest; 3) a transition reach that changes the flow toward sub-critical conditions; 4) super-critical flow along the chute; 5) a hydraulic jump in the energy dissipator due to an abrupt change from super-critical into sub-critical flow; and 6) sub-critical flow in the end channel (Erfanain-Azmoudeh and Kamanbedast, 2013; Wan *et al*., 2017).

Super-critical flow in the chute is marked by very high velocities. However, as the flow velocity increases, pressure decreases (Khatsuria, 2005; Kirkgoz, Akoz and Oner, 2010), consistent with the Bernoulli equation. Under these conditions, the vapour pressure may be reached, leading to the formation of vapour bubbles. These bubbles collapse when the flow moves into regions of higher pressure, causing surface damage (Sutopo, 2014; Bai, Wang and Zhang, 2018). Damage may expand as water pressure acts on the peeled surface, potentially developing into a cross-sectional cavity. Consequently, structural damage occurs (Falvey, 1990; Razos, Koutsoyiannis and Leandro, 2025). The process is known as the cavitation phenomenon.

Shear stress can be reduced when air is present in near-bed flow layer, which can also reduce the cavitation damage (Chanson, 1993). Self-aeration is the aeration of the free-surface flow, and the process has been studied since 1940s, for example by Volkart (1983), and Ervine and Falvey (1987). However, Chanson (1993) described factors influencing the aeration process, including the distribution of flow velocity, stress, and the size as well as concentration of air bubbles. The operating principle of an aerator was described by Kells and Smith (1990) as follows: an aerator installed in the channel bed forces air to enter the free surface flow and beneath the jet (Johnson and Savage, 2006). An aerator can be divided into four zones: approach zone, transition zone, aeration zone, and de-aeration zone. Aerator geometry determines the effectiveness of aeration (Wan, Liu and Rasa, 2018; Catucci, Briganti and Heller, 2021).

This research intends to investigate one spillway in Indonesia, especially a spillway with a chute that has a stepped bed slope. Flow is analysed numerically using the CFD method in Ansys Fluent to identify the cavitation potential and to assess the impact of additional aeration.

## MATERIALS AND METHODS

### RESEARCH LOCATION

This research focuses on the development of aerator dimensions and was conducted at the spillway of Tigadihaji Dam, located on the Selabung River within the Musi-Banyuasin River Region. The dam is situated in Sukabumi Village, Tigadihaji District, Ogan-Komering Regency-Ulu (South OKU)-South Sumatera Province-Indonesia, at approximately 4°37'44.154"S and 103°52'36.748"E.

### DATA

The spillway of Tigadihaji Dam is an open-channel spillway with a total length of 769.7 m. It includes a stepped chute with four different slopes, as shown in Figure 1a. In this research, a partial model of the spillway channel was developed, covering chute-3 and 4, and a ski-jump energy dissipator. The channel section from chute-3 to the ski-jump is rectangular channel with a width of 35.5 m and a height of 4.5 m. The bed slope is 1: 35 for chute-3 and 1: 1.5 for chute-4. The initial bed elevation is +230.86 m and the lowest elevation on the ski-jump is +198.00 m. The design discharge for chute corresponds to the 1000-year return period design flood and it is about 1,154.30 $m^3 \cdot s^{-1}$.

The numerical model was developed in a three-dimensional (3D) configuration, as shown in Figure 1b, with a total length of 227.4 m and a width of 35.0 m. The boundary conditions of this model were defined as follows: the inflow boundary was located at the beginning of chute-3, the outflow boundary at the end of the ski-jump, and the upper boundary at the spillway wall crest.

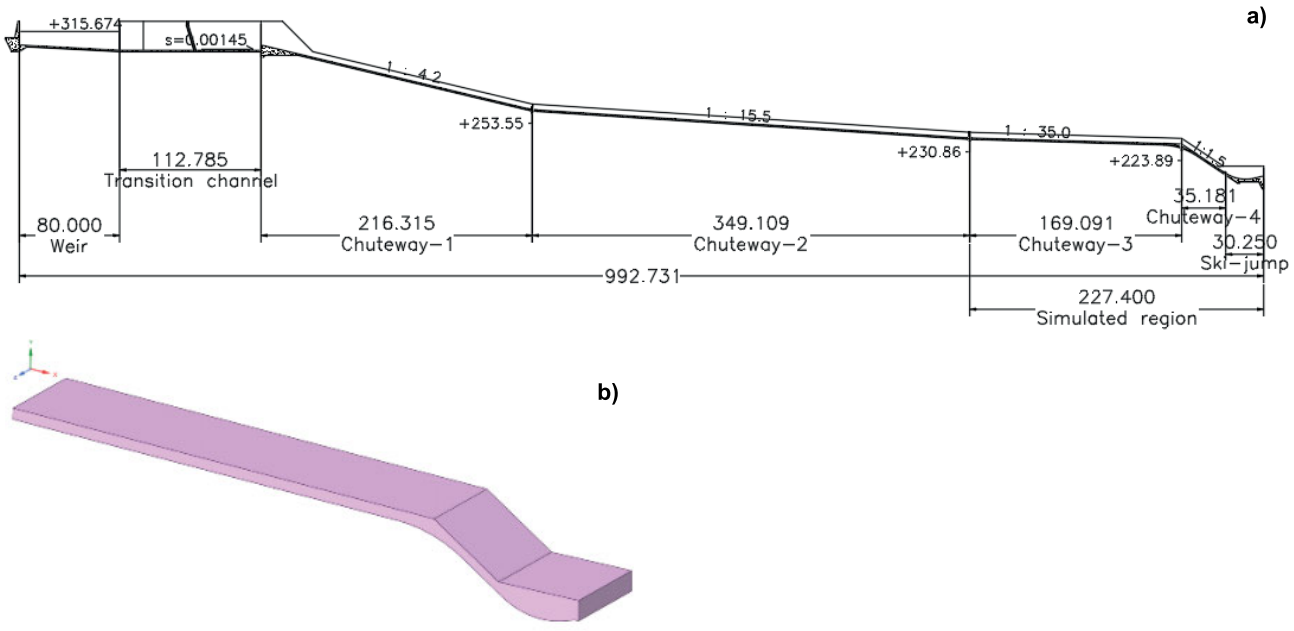


**Fig. 1.** Geometry and three-dimensional computational fluid dynamics (CFD) model of spillway (series 0 – without aerator): a) long section, b) model of 3D CFD; source: own elaboration

Then, this model was discretised into a mesh using an element size of 500 mm. The input data to Ansys Fluent consists of boundary condition, fluid that is used, method of analysis, etc. as presented in Table 1.

**Table 1.** Input on Ansys Fluent simulation

| Parameter | Value for discharge scenarios | | | |
|---|---|---|---|---|
| | $Q_2$ | $Q_{100}$ | $Q_{1000}$ | $Q_{PMF}$ |
| Inlet condition (flow rate) ($m^3 \cdot s^{-1}$) | 501.07 | 947.49 | 1154.3 | 3487.64 |
| Water height inlet (m) | 1.010 | 1.250 | 1.462 | 3.375 |
| Outlet condition (pressure outlet) | 101,325 Pa | | | |
| Time | transient (time step 0.01 s) | | | |
| Fluid | water and air | | | |
| Gravitation | 9.81 $m \cdot s^{-2}$ ($y$-axis) | | | |
| Model | volume of fluid | | | |

Explanations: $Q_2$ = 2-year return period flood discharge, $Q_{100}$ = 100-year return period flood discharge, $Q_{1000}$ = 1000-year return period flood discharge, $Q_{PMF}$ = probable maximum flood discharge.
Source: own study.

## EVALUATION ON THE POTENCY OF CAVITATION

The prediction of cavitation event can be obtained by using the cavitation number ($s$) on Equation (1):

$$\sigma = \frac{P_0 - P_v}{\frac{\rho v_0^2}{2}} \quad (1)$$

$$P_0 = P_a + P_g \quad (2)$$

where: $P_0$ = reference pressure at the flow location (kPa), $P_v$ = water vapour pressure at the operating temperature (kPa), $\rho$ = density of water ($kg \cdot m^{-3}$), $v_0$ = local flow velocity ($m \cdot s^{-1}$), $P_a$ = atmospheric pressure (101 kPa), $P_g$ = local pressure (kPa).

Cavitation risk along the spillway surface was evaluated based on the cavitation number ($\sigma$). According to the classification proposed by Falvey (1990), flow conditions with $\sigma > 1$ are generally considered safe and unlikely to cause cavitation damage. When the cavitation number decreases to values between approximately 0.6 and 1.0, the risk of cavitation initiation becomes low and is typically associated with light cavitation. For $\sigma$ values of about 0.4 to 0.6, moderate cavitation damage may occur. A higher cavitation risk is expected when $\sigma$ falls between 0.2 and 0.4, while values lower than 0.2 indicate a very high cavitation risk and potentially severe structural damage.

The cavitation number was evaluated at the 16 review points shown in Figure 2a (points A–P). Velocity was measured at these review points, with measurement taken at the channel bed. Figure 2b shows the locations of the pressure measurement points used for model validation (points 7–11).

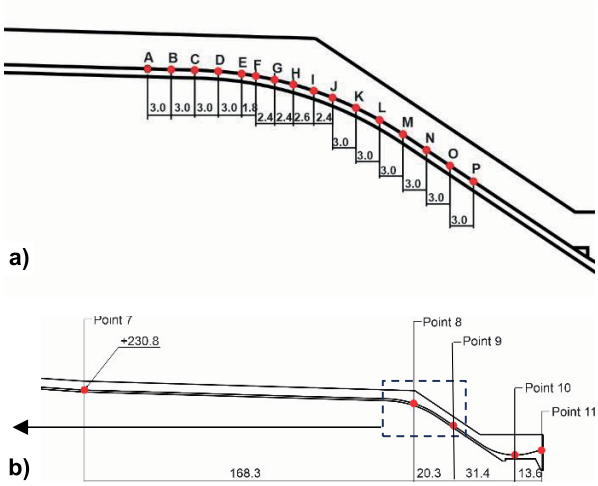


**Fig. 2.** Location of review points on the longitudinal section of model: a) measurement points on series 0 and series 1, b) measurement points for model validation; source: own elaboration

# RESULTS AND DISCUSSION

## FLOW SIMULATION SCENARIOS

Flow simulations for series 0 and series 1 were conducted for return periods of 2 years, 1000 years, and the probable maximum flood (PMF). However, the design consideration is based on the spillway design flood, $Q_{1000}$ = 1,154.3 $m^3 \cdot s^{-1}$. The series 0 model is presented in Figure 1b, and the series model 1 includes an additional aerator.

## MODEL VALIDATION

The computational fluid dynamics (CFD) model validation was performed by comparing the results of CFD model simulation of series 0 and the physical model that has been carried out by the Laboratory of Hydraulics and Water Geo-Technical Institution in Bandung in 2022. The validation followed the flow simulation on the design flood of $Q_2$, $Q_{100}$, $Q_{1000}$ and $Q_{PMF}$. A physical model was constructed at an undistorted scale of 1:50. The model represents a prototype area of 294.5 $m^2$ (corresponding model area: 117.8 $m^2$) and includes the spillway, main dam, and a portion of inundation reach extending approximately 270 m from the spillway upstream. The total prototype length represented in the model is 992 m. The flow simulation was carried out by supplying a discharge scaled according to the model scale. Pressure was measured using piezometers at 11 locations. However, discharge was measured downstream of the spillway physical model using Thomson measuring device. Comparison between the physical model and the prototype indicated that the model is sufficiently similar, with a nonconformity value of less than 1%. Likewise, the discharge flow data from the physical model are sufficiently similar to the prototype design, with a nonconformity value of less than 5%.

The test results of spillway physical model show that the flow on the chute is relatively uniform. Piezometer readings (Tab. 2) at points 4, 8, and 11 for the PMF discharge indicate negative pressures greater than 4 m. Therefore, it is recommended to add a pressure-relief channel. The pressure measurement results are presented in Table 3, with the analysis focused on

**Table 2.** Reading result of piezometer on the physical model for points 1–11

| Discharge | Value in point | | | | | | | | | | |
|---|---|---|---|---|---|---|---|---|---|---|---|
| | 1 | 2 | 3 | 4 | 5 | 6 | 7 | 8 | 9 | 10 | 11 |
| $Q_2$ | 0.55 | 0.20 | 6.25 | 1.30 | 1.40 | 2.25 | 1.00 | −0.10 | −0.10 | 1.15 | −4.9 |
| $Q_{100}$ | 0.00 | 0.25 | 7.50 | 1.65 | 2.50 | 4.75 | 2.25 | −1.15 | 0.15 | 4.90 | −5.5 |
| $Q_{1000}$ | −0.30 | 0.30 | 8.25 | 0.85 | 2.25 | 5.40 | 2.05 | −1.35 | −0.40 | 3.80 | −5.2 |
| $Q_{PMF}$ | −0.50 | 9.00 | 8.75 | −9.75 | 4.45 | 11.65 | 5.00 | −5.25 | 1.00 | 24.50 | −7.8 |

Explanations as in Tab. 1.
Source: Balai Hidrologi dan Geoteknik Keairan (2022).

the points 7 to 11. The data show that the pressure distribution varies, and negative pressure generally occurs in areas where the geometry changes. The pressure at point 7 tends to increase as the discharge increases. At this location, the chute profile forms a curve-upward vertical curve. Accordingly, the pressure at point 7 increases with increasing discharge, in accordance with the chute geometry at that point. In contrast, at point 8, the pressure is negative and becomes more negative as the discharge increases, which coincides with a concave-downward vertical curve profile. This finding is consistent with the research of Bagherzadeh, Ghaeini-Hessaroeiyeh and Fadaei-Kermani (2025), who reported that a pressure decrease to negative values under similar geometric conditions. At point 8, the pressure increases proportionally with the additional discharge.

The local pressures at the review points from 7 to 11 show physical-model and CFD values ranging from −8.2 to 27.0. The pressure trend in the CFD model is similar to that in the physical model, although the values differ, as presented in Figure 3. The deviation is relatively large for the $Q_{PMF}$ simulation, with a pressure difference of 2.5 m $H_2O$. However, for the design flood of $Q_2$, the maximum pressure difference is 1 m $H_2O$. For the design floods $Q_{100}$ to $Q_{1000}$, the pressure difference is 8 m $H_2O$.

## MODEL OF SERIES 0

The determination coefficient ($R^2$) is 0.97 and the root mean square error (*RMSE*) is 1.105, indicating that the CFD simulation matches the physical data with high accuracy and a small relative error compared with the data range. These results indicate that the CFD model is reliable and feasible for analysing other scenarios, including extreme-discharge conditions, and has potential for further development in future simulations.

The flow simulation for series 0 shows a significant development of the flow profile with increasing discharge, as presented in Figure 4a. At low discharge ($Q_2$), the flow is thin and stable, while at high discharge ($Q_{1000}$ and $Q_{PMF}$), the flow

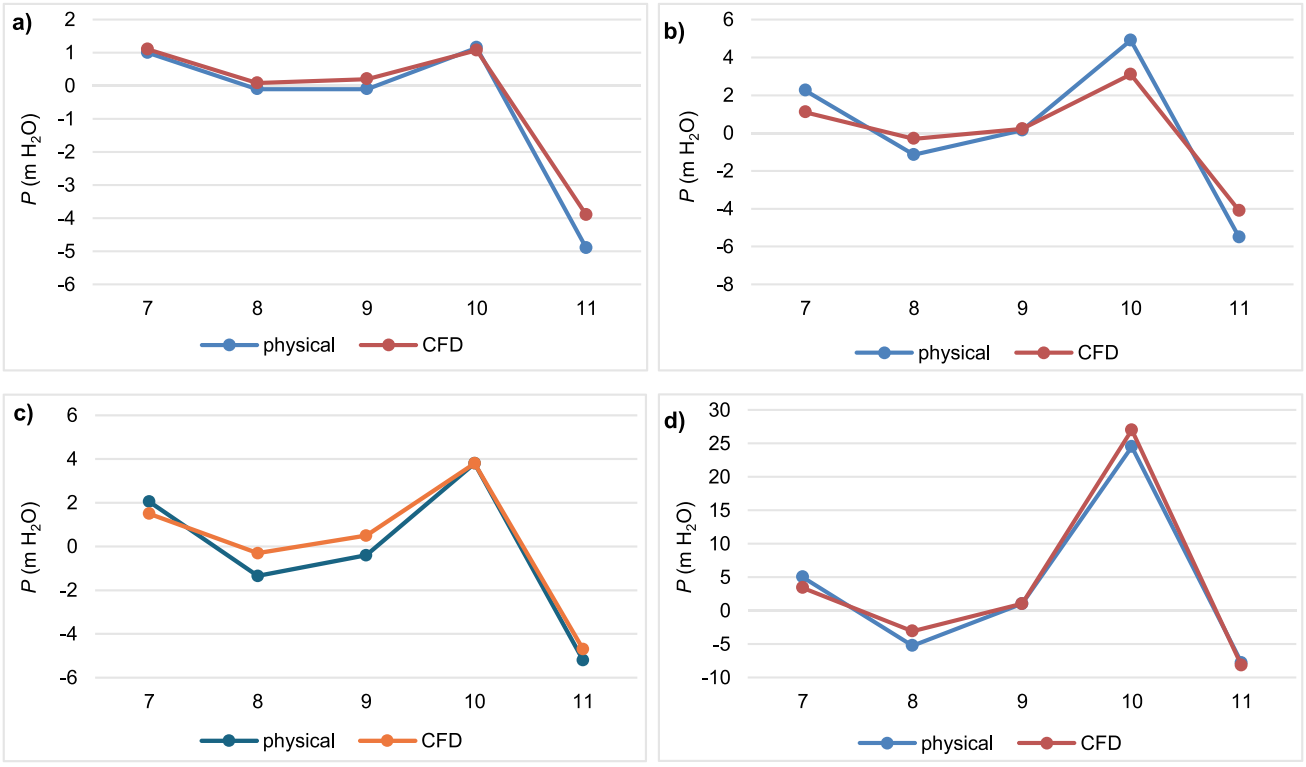


**Fig. 3.** Pressure (*P*) on points 7–11 of physical model and computational fluid dynamics (CFD) at simulations of different discharges: a) 2-year return period flood discharge ($Q_2$), b) 100-year return period flood discharge ($Q_{100}$), 1000-year return period flood discharge ($Q_{1000}$), probable maximum flood discharge ($Q_{PMF}$); source own study

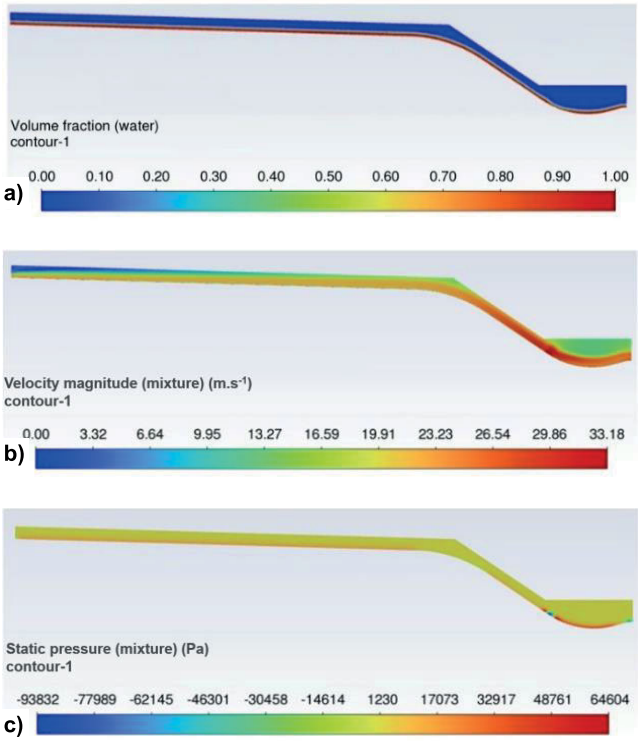


**Fig. 4.** Simulation result on series 0 of 1000-year return period flood discharge ($Q_{1000}$): a) contour profile of water-air volume fraction, b) contour profile of velocity, c) contour profile of pressure; source: own study

becomes thicker and more turbulent due to the dominance of the water-air two-phase flow. Super-critical flow occurs at all discharges, with a Froude number (F) > 1, indicating low pressure potential and a risk of cavitation. In the stilling basin, the flow pattern changes from calm to unstable due to back water interaction at high discharge.

The velocity distribution from chute-3 to the energy dissipator is presented in Figure 4b. The highest velocities occur at chute-4, which is steeper, and the flow vectors show vortex formation at high discharge. Channel velocity increases with increasing discharge, as shown by the measured velocities at points A to P presented in Figure 5a.

The pressure along channel in Figure 4c fluctuates. The highest pressure accumulates at the chute bed and dissipator; however, negative pressure is identified at points with flow acceleration or geometric changes, such as the concave vertical-curve profiles of chute-3 and 4, the chute block, and the end of the ski-jump. This condition shows a significant potential for cavitation and should be addressed in the design, mainly in the slope transition zone and at the end of the spillway.

The assessment of cavitation potential in the physical model, based on the pressure measurements, produced values of −1.35 ($Q_{1000}$) and −5.25 ($Q_{PMF}$) at point-8 (Tab. 2). In the CFD model, pressure was assessed at points A to P, and the result are presented in Figure 5b. The lowest pressure was −29,950 Pa at point K under the $Q_{PMF}$ condition and −3,483 Pa under $Q_{1000}$. Under the lowest discharge ($Q_2$), the lowest pressure was 1,037 Pa.

## MODEL OF SERIES 1

The series 1 model is the same as the series 0 model, with the addition of an aerator. Figure 6a shows the aerator installed at the meeting junction of chute-3 and 4, at a distance of about 10 m from the point of the lowest pressure.

The ramp–offset aerator with air ducts on both sidewalls was selected due to its simple geometry and ease of construction. The aerator was installed at the transition section where the chute slope changes from 1:35 to 1:1.5, allowing effective air entrainment into the lower flow layers. The deflector ramp diverts the high-velocity flow upward, forming a cavity downstream, while the offset provides additional space for air entrainment and mixing beneath the jet, helping to prevent cavitation damage on the concrete surface (Chanson, 1993; Novakoski *et al.*, 2020). The side air ducts are connected to the atmosphere and supply air to the cavity region below the jet, ensuring stable aeration and preventing negative pressure peaks (Chanson, 1993; Pfister and Hager, 2011). The dimensions of aerator are illustrated in Figure 6b: ramp ($q$) = 6.38°, slope of the channel bed ($a$) = 18.4°, ramp height ($t_r$) = 31 mm, offset depth ($ts$) = 0.5 m, air duct length ($L_d$) = 1 m, and air duct width ($b_d$) = 0.5 m.

The flow profile along the series 1 channel is similar to that of series 0. The channel capacity is sufficient with no run-off from $Q_2$ to $Q_{1000}$. The flow thickness from chute 3 gradually decreases as it passes through chute 4. After passing the aerator, no jump occurs. The flow layer in the channel bed is shown in Figure 7a. For the $Q_{PMF}$ simulation, chute 3 is still able to convey the flow well; however, run-off is identified in several sections of chute 4.

The flow profile surrounding the aerator is clearly shown in Figure 7a, particularly in the offset area. The water fraction

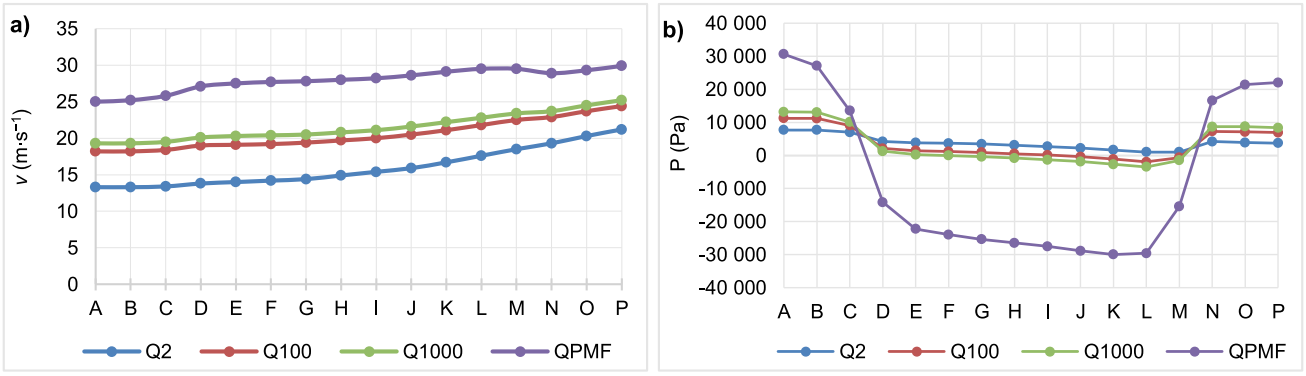


**Fig. 5.** Velocity ($v$) and pressure ($P$) on the monitoring point of A–P, series 0: a) velocity, b) pressure; $Q_2$, $Q_{100}$, $Q_{1000}$, and $Q_{PMF}$ as in Tab. 1; source: own study

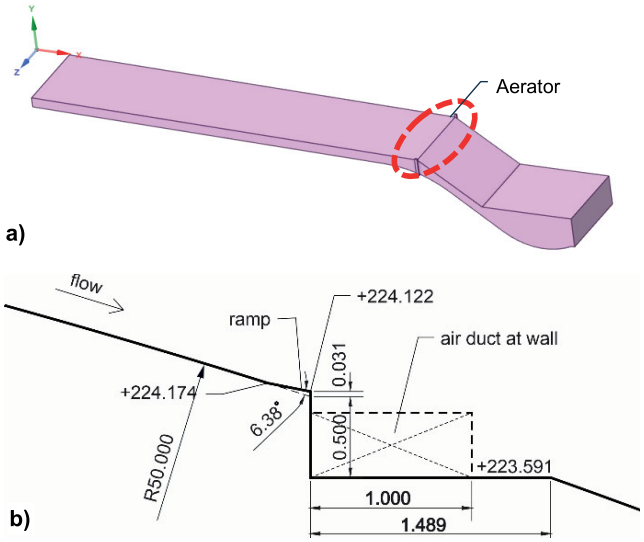


**Fig. 6.** Aerator configuration and geometric details of the air duct: a) 3D-model of series 1, b) and longitudinal section with geometric parameters of aerator; source: own study

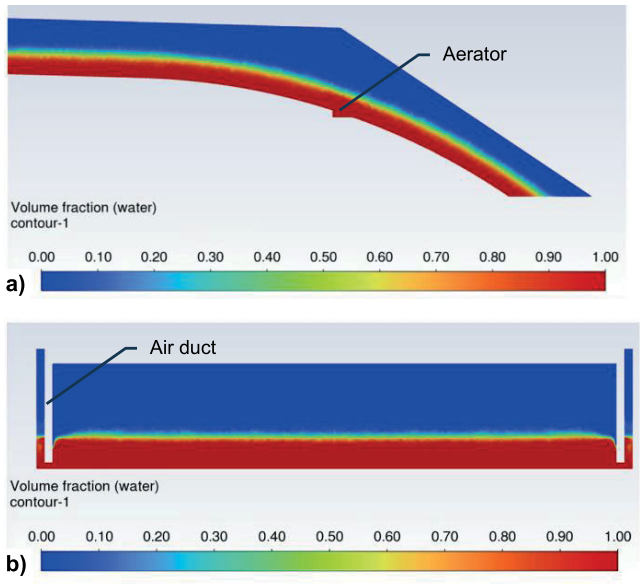


**Fig. 7.** Fraction profile of water-air volume on aerator area, series 1 of 1000-year return period flood discharge ($Q_{1000}$): a) long section of aerator, b) long section of air duct; source: own study

is close to 1, mainly in the channel bed, indicating that the area is dominated by water flow. The same condition is also observed in the air duct below, as presented in Figure 7b, where the duct is filled with water to a depth that almost equivalent with the flow depth in the channel. The simulation results show that installing the ramp and offset aerator at the slope of the channel bed from 1:35 to 1:1.5 produces a submerged aerator condition. Under this configuration, the flow remains attached to the channel surface after passing the aerator; therefore, air cannot enter the channel effectively. This phenomenon indicates that the combination of aerator type and installation location has not been optimal for creating the air voids needed to prevent cavitation.

Generally, the flow simulation results show that flow velocity increases with increasing discharge, as indicated by the recorded velocity curve in Figure 8a, for simulations from $Q_2$ to $Q_{PMF}$. Figure 9a shows the longitudinal velocity contour profile around the aerator and shows that the flow velocity upstream of the aerator continues to increase after passing the aerator. The contour colours show that surface velocity is higher than the flow velocity near the channel bed. The flow aligned with the surface experiences a reduction in velocity when passing the offset and then increases again downstream.

This pattern is clearly illustrated by the measured data in Figure 8a. The flow velocity at point H (before the offset) is about 21 $m \cdot s^{-1}$, decreasing to 20.1 $m \cdot s^{-1}$ at point I (after the offset), then increasing to 20.4 $m \cdot s^{-1}$ at point J (about 1.7 m downstream of the offset), and returning to 21 $m \cdot s^{-1}$ at point K. In addition, a colour difference is visible in the offset area, indicating a zone of very low velocity, close to zero, where a water fraction is present. The local pressure distribution based on the contour in Figure 9b for chutes 3 and 4 under $Q_2$, $Q_{1000}$, and $Q_{PMF}$ shows an irregular pressure distribution along the channel. In general, pressure decreases downstream. Lower pressure is identified near the channel back area, as shown by the brighter contour gradation, whereas higher pressure is concentrated around the offset section.

Based on the measured data presented in Figure 8b, the local pressure for the $Q_{1000}$ simulation at points F to M are negative, ranging from −149 to −3,891 Pa, except at point I, which is located at the aerator. However, at the other measured points it is positive. The visualisation in Figure 9a shows that along chutes 3 and 4, pressure decreases mainly in the slope transition area of the channel bed. The contour shows that the pressure is relatively higher around the offset than in the upstream and downstream sections.

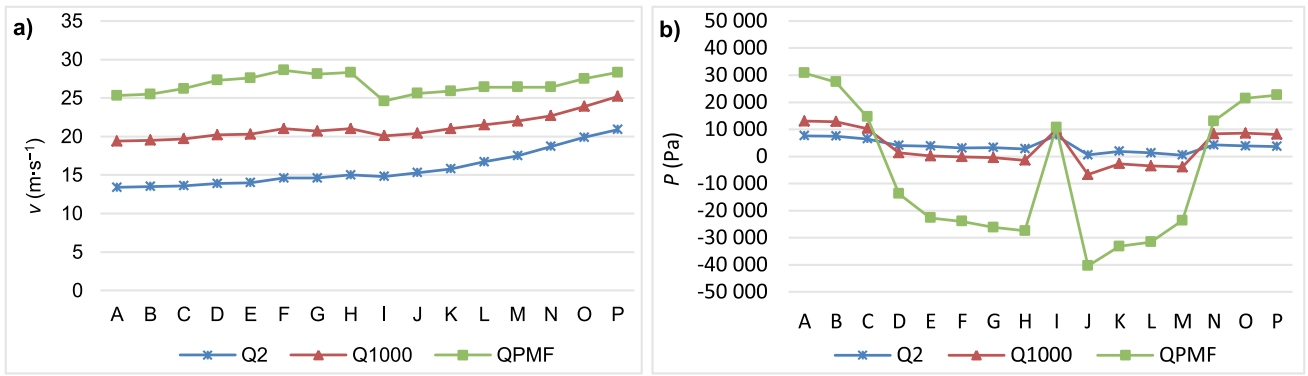


**Fig. 8.** Hydraulic characteristics along the spillway for series 1 on the review point of A–P: a) velocity ($v$), b) pressure ($P$); $Q_2$, $Q_{1000}$, and $Q_{PMF}$ as in Tab. 1; source: own study

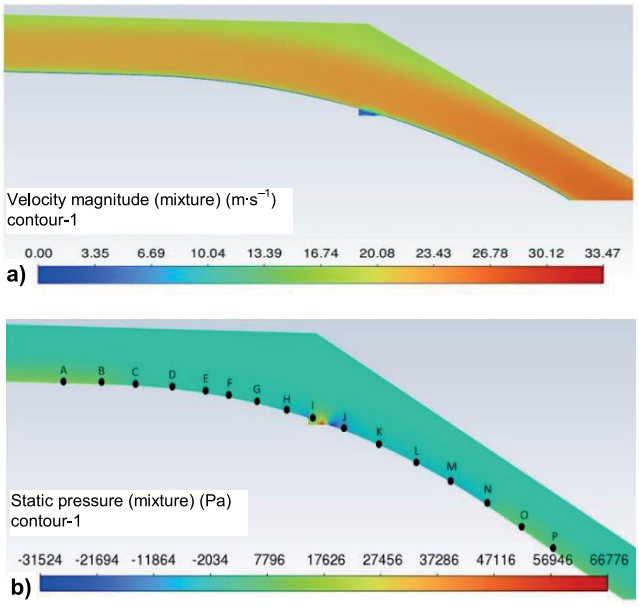


**Fig. 9.** Simulation result on series 1 of 1000-year return period flood discharge ($Q_{1000}$): a) contour profile of velocity, b) contour profile of pressure; source: own study

Although an aerator is installed, the recorded minimum pressure is lower than in the condition without an aerator (series 0). The minimum pressure with the aerator is −6,733 Pa at point J, whereas in series 0 it is −1,855 Pa. This indicates that the ramp-offset causes a significant pressure decrease due to the sudden geometric change. However, the aeration process does not occur effectively; therefore, an increase in pressure is not achieved.

## DISCUSSION

As shown in Figure 10b, the added aerator consistently produces a significant increase in local pressure around the installation point, mainly at point I. Meanwhile, at the other points, the pressure difference between the condition without aerator (series 0) and with an aerator (series 1) is relatively small. It indicates that the aerator effect is local. Based on the Figure 7, the offset area is inundated with water, which obstructs the air entrainment process. As a result, no pressure increase occurs downstream of the aerator, as expected in the design of an effective aeration system.

Generally, the cavitation index ($\sigma$) increases at most points in series 1, as shown by the curve in Figure 11, indicating an improvement in cavitation potential. The most significant increase occurs at point I, where $\sigma$ rises from 0.428 (series 0) to 0.527 (series 1), while the risk remains moderate. However, at several locations the cavitation index does not change significantly. In particular, at point P, the cavitation index remains approximately 0.33, and the cavitation risk remains high. In addition, $\sigma$ at point O increases only slightly from 0.351 to 0.368, and remains in the high risk category. In contrast, notable improvement occurs at points K and L, where the cavitation index increases from values within the high-risk range in series 0 to values exceeding 0.4 in series 1, reducing the cavitation risk to the moderate category. The impact of the added aerator on increasing $\sigma$ extends from point I (aerator location) to point O, about 20 m away; at point P, about 23.5 m away, there is no influence on $\sigma$.

After carrying out flow simulations for both models – series 0 (chute without an aerator) and series 1 (chute with a ramp-offset aerator) – the impact of the added aerator on the predicted cavitation risk potential can be identified. In series 0, the risk potential is moderate from points A to J, while high risk occurs from point K to P.

The cavitation index is influenced by local pressure and velocity. The $\sigma$ curve in Figure 11 and the velocity curve in Figure 11 illustrate the impact of velocity changes on $\sigma$. Aerator installation causes a decrease in flow velocity downstream, and although changes in local pressure downstream of the aerator are very small, $\sigma$ increases downstream. The simulation shows that when the deflector is submerged and the jet remains attached to the chute surface, downstream velocity gradually decreases as part of the kinetic energy is converted into pressure. This condition weakens aeration and limits air entrainment. Similar findings were reported by Kökpınar and Göğüş (2002), who observed that the absence of jet separation reduced acceleration and caused a local velocity drop, and by Pfister, Hager and Asce (2010), who noted that low deflector height relative to flow depth results in attached flow with reduced velocity due to energy loss in the reattachment zone. Consistent with these studies, the present results indicate that the velocity increases only near the deflector ramp before gradually diminishing downstream.

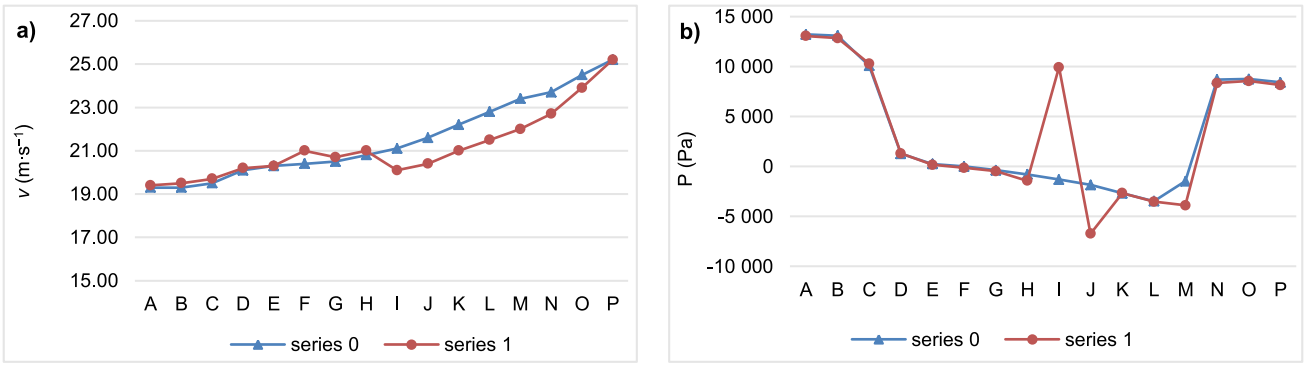


**Fig. 10.** Simulation result on A–P, series 0 and series 1 of 1000-year return period flood discharge ($Q_{1000}$): a) velocity ($v$), pressure ($P$); source: own study

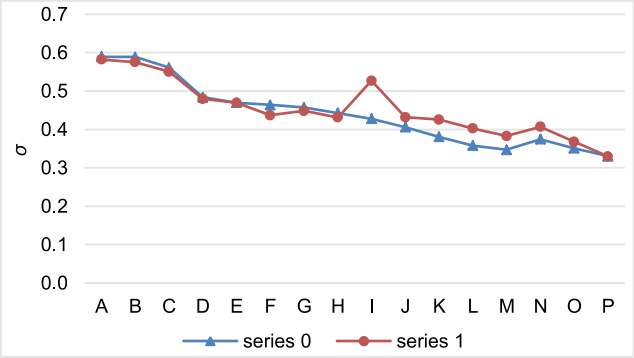


**Fig. 11.** Cavitation index ($\sigma$) on the A–P points, 1000-year return period flood discharge ($Q_{1000}$); source: own study

## CONCLUSIONS

The computational fluid dynamics (CFD) modelling of the spillway for series 0, covering the reach from chute 3 to the energy dissipator, provides information on local pressure and velocity measured at 16 monitoring points. These parameters are then used to analyse the cavitation index ($\sigma$). For the simulation of 1000-year return period flood discharge ($Q_{1000}$), chute 3 shows a moderate cavitation risk, whereas chute 4 shows a high cavitation risk.

The series 1 simulation was conducted to evaluate the impact of chute-based aeration on $\sigma$. Based on the results and discussion above, the conclusions are as follows: 1) adding a deflector-offset aerator at the chute slope transition from 1: 35 to 1:1.5 increases the cavitation index ($\sigma$), with a maximum increase of 0.1. The increase in $\sigma$ extends approximately 20 m downstream of the aerator; 2) placing an offset-type aerator on the less steep arched profile is not optimal because the aeration process is not smooth, and the offset section is inundated with water; and 3) overall, the aerator successfully reduces the cavitation risk level at several critical points; however, the design still needs to be optimised to produce more uniform protection along all streamlines.

## CONFLICT OF INTERESTS

All authors declare that they have no conflict of interests.

## REFERENCES

Amador, A., Sánchez-Juny, M. and Dolz, J. (2006) "Characterization of the non-aerated flow region in a stepped spillway by PIV," *Journal of Fluid Engineering*, 128(6), pp. 1266–1273. Available at: https://doi.org/10.1115/1.2354529.

Bagherzadeh, S., Ghaeini-Hessaroeiyeh, M. and Fadaei-Kermani, E. (2025) "Prediction of cavitation damage using SVM model based on air–water two-phase flow over dam spillway," *Applied Water Science*, 15, 70. Available at: https://doi.org/10.1007/s13201-025-02406-4.

Bai, R. *et al.* (2019) "Experimental investigation of bubbly fow and air entrainment discharge downstream of chute aerators," *Journal of Environmental Fluid Mechanics*, 19, pp. 1455–1468. Available at: https://doi.org/10.1007/s10652-019-09667-z.

Bai, Z., Wang, Y. and Zhang, J. (2018) "Pressure distributions of stepped spillways with different horizontal face angles," *Proceedings of the Institutionof Civil Engineers – Water Management*, 171(6), pp. 299–310. Available at: https://doi.org/10.1680/jwama.16.00093.

Balai Hidrologi dan Geoteknik Keairan (2022) *Laporan akhir uji model hidraulik pelimpah bendungan Tiga Dihaji, Kabupaten Ogan Komering Ulu Selatan – Sumatera Selatan [Final report of hydraulic model test of Tiga Dihaji Dam spillway, South Ogan Komering Ulu Regency – South Sumatra]*. Jakarta: Direktorat Jenderal Sumber Daya Air, Kementerian Pekerjaan Umum dan Perumahan Rakyat.

Catucci, D., Briganti, R. and Heller, V. (2021) "Numerical validation of novel scaling laws for air entrainment in water," *Proceedings of the Royal Society A*, 477(2255), 20210339. Available at: https://doi.org/10.1098/rspa.2021.0339.

Chanson, H. (1993) "Self-aerated flows on chutes and spillways," *Journal of Hydraulic Engineering*, 119(2), pp. 220–243. Available at: https://doi.org/10.1061/(ASCE)0733-9429(1993)119:2(220).

Departemen Pekerjaan Umum, Direktorat Jenderal Pengairan, Direktorat Bina Teknik (1999) *Panduan perencanaan bendungan urugan. Vol. IV Desain bangunan pelengkap [Design guidance of earthfill dam. Vol. IV Design of completion structure]*. Jakarta. Available at: https://www.scribd.com/document/480978984/PANDUAN-PERENCANAAN-BEND-URUGAN-VOL-4-DE-SAIN-BANGUNAN-PELENGKAP-pdf (Accessed: August 10, 2025).

Environment Agency (2022) *Spillway design guide. FCERM Research & Development Programme Research report*. Bristol. https://assets.publishing.service.gov.uk/media/62b32702d3bf7f0afc388104/Spillway_Design_Guide_1.pdf (Accessed: August 10, 2025).

Ebrahimnezhadian, H. and Manafpour, M. (2021) "Study of two-phase flow behaviour around chute aerator using open FOAM," *International Journal on Advanced Science Engineering Information Technology*, 11(4), pp. 1574–1581. Available at: https://doi.org/10.18517/ijaseit.11.4.10197.

Erfanain-Azmoudeh, M.H. and Kamanbedast, A.A. (2013) "Determine the appropriate location of aerator system on gotvandoliadam's spillway using Flow 3D," *American-Eurasian Journal of Agriculture & Environmental Sciences*, 13(3), pp. 378–383. Available at: https://doi.org/10.5829/idosi.aejaes.2013.13.03.458.

Ervine, D.A. and Falvey, H.T. (1987) "Behaviour of turbulent water jets in the atmosphere and in plunge pools," *Proceedings of the Institution of Civil Engineers*, P. 2, 83(1), pp. 295–314. Available at: https://www.sci-hub.in/10.1680/iicep.1987.353 (Accessed: August 10, 2025).

Falvey, H. (1990) "Cavitation in chutes and spillways," *Engineering Monograph*, 42. https://www.usbr.gov/tsc/techreferences/computer%20software/software/EM42/EM42.pdf (Accessed: August 10, 2025).

Johnson, M.C. and Savage, B.M. (2006) "Physical and numerical comparison of flow over ogee spillway in the presence of tailwater," *Journal of Hydraulic Engineering*, 132(12), pp. 1353–1357. Available at: https://doi.org/10.1061/(ASCE)0733-9429(2006)132:12(1353).

Julien, P.Y., Kositgittiwong, D., and Chinnarasri, C. (2014) "Model of flow over spillways by computational fluid dynamics," *Water Management*, 167(3), pp. 164–175. Available at: https://doi.org/10.1680/wama.12.00034.

Kells, J.A., and Smith, C.D. (1990) "Reduction of cavitation on spillways by induced air entrainment," *Canadian Journal of Civil*

*Engineering*, 18, pp. 358–377. Available at: https://doi.org/10.1139/l91-047.

Khatsuria, R.M. (2005) *Hydraulics of spillway and energy dissipator*. New York: Marcel Dekker. Available at: https://api.pageplace.de/preview/DT0400.9780203996980_A24397967/preview-9780203996980_A24397967.pdf (Accessed: August 10, 2025).

Kirkgoz, M.S., Akoz, M.S. and Oner, A.A. (2010) "Numerical modeling of flow over a chute spillway," *Journal of Hydraulic Research*, 47(6), pp. 790–797. Available at: https://doi.org/10.3826/jhr.2009.3467.

Kökpınar, M.A. and Göğüş, M. (2002) "High-speed jet flows over spillway aerators," *Canadian Journal of Civil Engineering*, 29(6), pp. 885–898. Available at: https://doi.org/10.1139/l02-088.

Kubrak, E. and Kubrak, J. (2022) "Practical aspects of the use of the sluice gate discharge equations to estimate the volumetric flow rate in the irrigation channels," *Journal of Water and Land Development*, 55, pp. 129–137. Available at: https://doi.org/10.24425/jwld.2023.148455.

Kubrak, J., Kubrak, E. and Binio, J.E. (2024) "The calibration of sharp-crested weirs with a horizontal edge used for measuring flows in partially full pipes," *Journal of Water and Land Development*, 60, pp. 24–31. Available at: https://doi.org/10.24425/jwld.2023.148455.

Kumcu, S.Y. (2017) "Investigation of flow over spillway modeling and comparison between experimental data and CFD analysis," *KSCE Journal of Civil Engineering*, 21(3), pp. 994–1003. Available at: https://doi.org/10.1007/s12205-016-1257-z.

Luna-Bahena, J.C. *et al.* (2018) "Experimental investigation of artificial aeration on a smooth spillway with a crest pier," *Water*, 10(10), 1383. Available at: https://doi.org/10.3390/w10101383.

Nasrabadi, M. and Aminpour, Y. (2020) "Numerical simulation of flow over stepped spillways with varying step-angle," *Hydro Science & Marine Engineering*, 2(2), pp. 20–28.

Novakoski, C.K. *et al.* (2020) "Stepped spillway with pre-aeration by a deflector: Flow characteristics," *Revista Brasileira de Recursos Hídricos (RBRH) / Brazilian Journal of Water Resources*, 25, e26. Available at: https://doi.org/10.1590/2318-0331.252020190051.

Pfister, M. and Hager, W.H. (2011) "Chute aerators: Steep deflectors and cavity subpressure," *Journal of Hydraulic Engineering*, 137(10), pp. 1208–1215. Available at: https://doi.org/10.1061/(ASCE)HY.1943-7900.0000436.

Pfister, M., Hager, W.H. and Asce, F. (2010) "Chute aerators. I: Air transport characteristics," *Journal of Hydraulic Engineering*, 136 (6), pp. 352–359. Available at: https://doi.org/10.1061/(ASCE)HY.1943-7900.0000189.

Razos, E., Koutsoyiannis, D. and Leandro, J. (2025) "Stochastic-dynamics modeling of chute slabs under spillway flows," *Water*, 17(5), 621. Available at: https://doi.org/10.3390/w17050621.

Safiloo, F. *et al.* (2025) "Investigating flow characteristics in different types of chute spillway aerators," *ISH Journal of Hydraulic Engineering*, 31(4), pp. 686–706. Available at: https://doi.org/10.1080/09715010.2025.2515486.

Seo, I.W. *et al.* (2016) "Spillway discharges by modification of weir shapes and overflow surroundings," *Environmental Earth Sciences*, 75, 496. Available at: https://doi.org/10.1007/s12665-016-5407-x.

Sutopo, Y. (2014) *Kavitasi di dasar saluran curam [Cavitation in steep channel bed]*. Yogyakarta: Andi.

Trinh, M.T. *et al.* (2025) "Hydro-forming of U-shaped parts with branches," *Engineering, Technology & Applied Science Research*, 15(1), pp. 19226–19231. Available at: https://doi.org/10.48084/etasr.9227.

Volkart, P. (1983) "Air slots for flow aeration," *Mitteilungen der Versuchsanstalt für Wasserbau, Hydrologie und Glaziologie*, 66. Available at: https://ethz.ch/content/dam/ethz/special-interest/baug/vaw/vaw-dam/documents/das-institut/mitteilungen/1980-1989/066.pdf (Accessed: August 10, 2025).

Wan, H. *et al.* (2017) "Numerical simulation of hydrodynamics and reaeration over a stepped spillway by the SPH method," *Water*, 9(8), 565. Available at: https://doi.org/10.3390/w9080565.

Wan, W., Liu, B. and Raza, A. (2018) "Numerical prediction and risk analysis of hydraulic cavitation damage in a high-speed-flow spillway," *Hindawi Shock and Vibration*, 2018(1), 1817307, pp. 1–11. Available at: https://doi.org/10.1155/2018/1817307.

Yang, J., Teng, P. and Zhang, H. (2018) "Experiments and CFD modeling of high-velocity two-phase flows in a large chute aerator facility," *Journal of Engineering Applications of Computational Fluid Mechanics*, 13(1), pp. 48–66. Avaiable at: https://doi.org/10.1080/19942060.2018.1552201.

Zhang, X. *et al.* (2024) "Insights into the cause of the oroville dam spillway failure 2017, California," *Environmental Science and Pollution Research*, 31(14), pp. 21356–21369. Avaiable at: https://doi.org/10.1007/s11356-024-32462-3.